

QECOOOL: On-Line Quantum Error Correction with a Superconducting Decoder for Surface Code

Yosuke Ueno¹, Masaaki Kondo^{1,2}, Masamitsu Tanaka³, Yasunari Suzuki⁴, and Yutaka Tabuchi^{5, (a)}

¹Graduate School of Information Science and Technology, The University of Tokyo, Tokyo, Japan

²RIKEN Center for Computational Science, Hyogo, Japan

³Graduate School of Engineering, Nagoya University, Aichi, Japan

⁴NTT Secure Platform Laboratories, Tokyo, Japan

⁵Research Center for Advanced Science and Technology, The university of Tokyo, Tokyo, Japan

{ueno, kondo}@hal.ipc.i.u-tokyo.ac.jp, masami_t@nagoya-u.jp, yasanari.suzuki.gz@hco.ntt.co.jp, yutaka.tabuchi@riken.jp

Abstract—Due to the low error tolerance of a qubit, detecting and correcting errors on it is essential for fault-tolerant quantum computing. Surface code (SC) associated with its decoding algorithm is one of the most promising quantum error correction (QEC) methods. QEC needs to be very power-efficient since the power budget is limited inside of a dilution refrigerator for superconducting qubits by which one of the most successful quantum computers (QCs) is built. In this paper, we propose an online-QEC algorithm and its hardware implementation with SFQ-based superconducting digital circuits. We design a key building block of the proposed hardware with an SFQ cell library and evaluate it by the SPICE-level simulation. Each logic element is composed of about 3000 Josephson junctions and power consumption is about $2.78 \mu\text{W}$ when operating with 2 GHz clock frequency which meets the required decoding speed. Our decoder is simulated on a quantum error simulator for code distances 5 to 13 and achieves a 1.0% accuracy threshold.

Index Terms—Quantum Error Correction, SFQ logic

I. INTRODUCTION

Quantum computers (QCs) are becoming an attractive computing paradigm, as the number of implementable qubits increases. A QC with the largest number of qubits today has 53 qubits [1] while real-world problems typically need more qubits. For example, a 256-bit RSA cipher with Shor’s algorithm [18] requires about thousands of qubits. One of the challenges towards a rapid increase in the number of qubits is its high fragility of the quantum state due to decoherence and other noises, which necessitates error tolerance mechanisms. A topological error-correcting code and associated quantum error correction (QEC) mechanism are widely studied to detect/correct errors [17]. Since it is not possible to directly observe qubits to detect errors, observational quantum bits called *ancillary* qubits (*ancilla bits*) are equipped in addition to informational qubits. Decoding an error-correcting code with ancilla bits to find erroneous qubits is a non-trivial task and requires a large amount of computation.

One of the most promising QC implementations today is made up of superconducting qubits. To realize superconductivity and avoid thermal noise, they are operated in a cryogenic environment, especially at the effective temperature of a few millikelvin ranges. While qubits are located on the millikelvin layer of a dilution refrigerator, most of the other components, including a processing unit for QEC, are located on a much higher temperature layer or even outside the refrigerator. This forces a QC to have many cables between different temperature layers, increasing the hardware complexity and latency of QEC processes which is one of the main hindrances of QC scalability. Performing QEC near the superconducting qubits dramatically alleviates this problem. However, the power budget of lower temperature layers in the dilution refrigerators is very restricted, for example, only tens of μW and around 1W in the millikelvin and 4-K layer, respectively. Extraordinary low-power QEC processing is necessary.

One of the most feasible error-correcting codes for QEC is *surface code* (SC) [8]. Since decoding the SC accurately is an NP-hard problem, approximating algorithms such as minimum-weight perfect matching (MWPM) [7] is usually considered. As its computational complexity is still high, there have been proposed several low-cost decoders [2], [3], [11]. Although correcting informational qubit errors is treated by a matching problem on a 2-D SC plane, we need to extend it to a 3-D SC lattice to deal with ancilla bit measurement errors whose error rate is equal to or even higher than that of informational qubits. Ancilla bits should be measured multiple times, and stacking each result temporally creates a 3-D SC lattice, which can be decoded by ordinary decoding algorithms for the 2-D plane with slight modifications. However, computational and circuit complexity greatly increases.

In this paper, we propose a power-efficient Quantum Error Correction by On-Line decoding algorithm (QECOOOL) for 3-D lattice and its hardware implementation using superconducting digital circuits with single flux quantum (SFQ). Most of the prior decoders for 3-D matching problems or direct extension of 2-D algorithms require a completed 3-D SC, which means the decoding process is performed after all the measurements are done for one QEC step. We refer to this as *batch-QEC*. Instead of waiting for all the measurements, QECOOOL starts a QEC process for every obtained SC plane with several consecutive accumulated SC planes. We call this *online-QEC*. Since online-QEC can inherently achieve a shorter QEC cycle than batch-QEC, the number of qubit errors on a single decoding process is expected to be small, leading to higher error correction performance.

QECOOOL is implemented with a specialized hardware logic with a spike signal-based matching architecture implemented by SFQ logic to realize the online-QEC with ultra-low-power and low-latency. Since the semiconductor process technology of SFQ is not scalable as that of CMOS due to the necessity of constructing superconducting rings, a large number of memory blocks are not implementable. QECOOOL adopts a distributed architecture approach and area-efficient design with small registers.

The contributions of this paper are summarized as follows:

- We propose QECOOOL, an on-line decoding algorithm for SC on a 3-D lattice that has significantly lower complexity than the standard MWPM and previously proposed decoders at the cost of slight degradation of error correction performance.
- We design a power- and area-efficient SFQ decoder based on the above algorithm.
- We evaluate the power consumption and area of the design with a SPICE-based circuit simulator and show that our implementation can work at the 4-K layer with around 2,500 logical qubits.
- We evaluate the error correction performance of QECOOOL with a quantum error simulator.

^(a)Presently the author is with RIKEN Center for Emergent Matter Science.

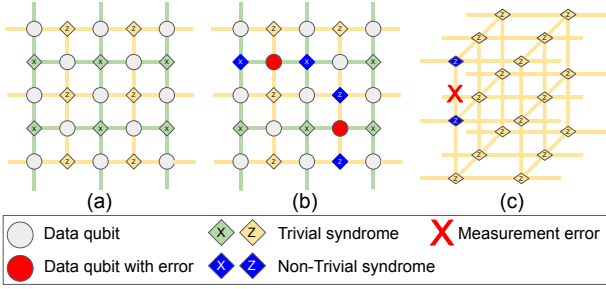


Fig. 1. Graphical illustration of surface code

The evaluation results show that QECool can perform sufficiently low-latency QEC while achieving very low-power consumption.

II. BACKGROUND AND RELATED WORK

A. Surface code

Surface code (SC) is a quantum error correction code that provides highly reliable QEC. Figure 1 shows the schematic view of a SC for code distance $d = 3$. It is implemented on a 2-D grid array of two types of physical qubits, data and ancilla qubits, which are represented as circles and squares in Fig. 1 (a), respectively. Data qubits are redundantly used to represent a single logical qubit. Ancilla qubits interact with their neighboring data qubits, and their measurements form the *error syndrome* (Fig. 1 (b)).

The purpose of decoding SCs is to find the types and location of qubit errors from error syndromes. There are two types of ancillary qubits, X - and Z -ancilla qubits, corresponding to Pauli- X (bit-flip) and Pauli- Z (phase-flip) error, respectively. Another error type, Pauli- Y error, is represented by combinations of X and Z errors. Each ancilla bit works as the parity of the number of errors on its four neighbors. Since ancilla qubits for X or Z errors are alternatively structured, decoding of SC can be independently performed for the X and Z -syndrome.

Decoding the SC is a process to find the most likely error correction operation from error syndromes. Since finding such an operation is NP-hard, it is common to reduce the problem's complexity to a polynomial-time solution by approximating a part of the problem. The most promising approach is applying the minimum-weight perfect matching (MWPM) problem [8]. A variety of decoders using machine learning [21], or union-find [3] have also been proposed.

Given that an ancilla bit measurement is susceptible to read errors, QEC needs multiple ancilla bit measurements over a series of quantum operations. This procedure creates multiple 2-D SC snapshots. By stacking them in the vertical direction, creating a 3-D lattice-shaped SC [4] as shown in Fig. 1 (c), error syndromes are detected by solving the matching problem on the 3-D lattice even with measurement errors.

B. Single Flux Quantum logic

The single flux quantum (SFQ) logic is a digital circuit that uses superconductor devices. Information processing in SFQ is performed with magnetic flux quanta stored in superconductor rings with Josephson junctions (JJs) that act as switching devices. The presence and absence of a single magnetic flux quantum ($\Phi_0 = 2.068 \times 10^{-15}$ Wb) represent logical '1' and '0', respectively. Several studies have shown SFQ-based microprocessor designs and demonstrated their ultra-high-speed and low-power operations [16]. However, more power efficiency is required to work with superconducting qubits in the same temperature layer.

C. Related Work on Hardware-Efficient Decoder

A union-find based surface code decoder is recently proposed and has attracted much attention because of its accuracy and simplicity [3].

A practical architecture for the union-find decoder is first proposed by Das et al. [2]. In their work, the fully pipelined hardware implementation contributed to the higher speed of the decoding process.

Using cryogenic computing as peripherals of QCs to perform controls, including QEC, has been actively studied [11], [19], [20]. Holmes et al. [11] designed a novel algorithm with SFQ to find quantum errors online for near-term quantum systems. In their work, multiple pairs of two flipped ancilla bits can be found in parallel to reduce the latency of the decoding process. They implemented a mechanism that makes "agreement" among ancilla bits to find pairs. Our base decoder algorithm is inspired by their mechanism but differs in the fact that QECool does not need the agreement mechanism to simplify the design. Moreover, none of the prior work addresses online-QEC on 3-D lattice for faster QEC cycle.

III. SPIKE-BASED ON-LINE QUANTUM ERROR CORRECTION

A. Base decoding algorithm

We first describe how to decode a SC on 2-D structures in QECool, which is inspired by the greedy algorithm of minimum-weight perfect matching problems [5]. The purpose of the decoder is to find pairs of erroneous ancilla bit locations such that the total Manhattan distance of all the pairs is minimized. We introduce a module named *Unit* associated with each ancilla bit. Each Unit is connected to neighboring four Units forming a 2-D grid structure as same as X or Z stabilizers. We also introduce a *Controller* module to orchestrate all the Units in a logical qubit.

QECool algorithm is shown in Algorithm 1. Though the algorithm shows online-QEC on a 3-D lattice, it can be considered as an algorithm for a 2-D plane if N_{depth} , the number of depth in the vertical direction (V-direction), and th_v , the maximum length or threshold in the V-direction to search for matchings, are set to 1 and -1, respectively. Each Unit has a unique row and column IDs originated by the Unit at the top-left corner. When each ancilla bit is measured, its value (0 and 1 indicate consistent and inconsistent for connected qubits, respectively) is stored into *Reg* on the associated Unit (MeasureEachUnit in Algorithm 1). In a QEC phase, the Controller assigns a Token to each Unit from the top-left (northwestern) corner. The decoding process shown in the "RestartUnit" procedure of Algorithm 1 is summarized as follows. Note that this procedure is supposed to be done in parallel in all the Units.

- 1) If a Unit gets the Token, it checks its own *Reg*. If it is 1, the Unit becomes the *sink* Unit and requests all the other Units to send a Spike toward the sink if their *Reg* is also 1, and then waits for the first Spike to come. If not, the Token is passed to the next Unit through the Controller.
- 2) When the Spike request comes to a non-sink Unit, it checks its own *Reg*. If *Reg* is 1, it initiates a Spike toward the sink Unit (Fig. 2(a)). The direction to send is determined locally by comparing its row ID and *currentRow* set by the Controller, and also *FlagToken* which indicates whether the Token is already passed in the past (see SPIKE procedure in Algorithm 1).
- 3) For a non-sink Unit with *Reg* value is 0, it may get a Spike from one of its neighboring Units. In this case, it passes the Spike to one of the other neighboring Units so that the Spike reaches the sink Unit. The direction to pass is determined in the same way as Step 2). It also calculates and saves the relative direction of the coming Spike by rotating 180 degrees of the incoming port's direction. This direction is used to generate an error syndrome in the following Step 4).
- 4) If the first Spike comes to the sink Unit, it generates a correct signal to an informational qubit on the coming Spike direction. It also sends *Syndrome* signal to that direction to correct errors

Algorithm 1 Spike-based on-line QEC for 3-D Surface code

```

1: MeasureEachUnit:
2:  $m = 0$ 
3: while true do
4:  $A = \text{checkAncilla}()$ 
5: if  $m = 0$  then
6:  $\text{Reg}[0] = A$ 
7: else
8:  $\text{Reg}[m] = \text{Reg}[m-1] \oplus A$ 
9: end if
10:  $m = m + 1$ 
11:  $\text{Sleep}(\text{Mcycle})$ 
12: end while

1: Controller:
2: start\_loop:
3: for  $C = 1$  to  $N_{limit}$  do
4: for  $b = 0$  to  $N_{depth}$  do
5:  $\text{shift} = \text{true}$ 
6: for  $i = 0$  to  $N_{row}$  do
7:  $\text{currentRow} = i$ 
8: for  $j = 0$  to  $N_{col}$  do
9: if  $m - b > th_v$  then
10:  $\text{giveToken}(i, j)$ 
11:  $\text{RestartUnit}(b)$ 
12: while  $!\text{getFinish}()$  &&  $!\text{Timeout}()$ 
13: end if
14:  $\text{shift} \& \& \text{Unit}(i, j).\text{Reg}[0]$ 
15: end for
16: end for
17:  $\text{sendResetFlag}()$ 
18: if  $\text{shift}$  then
19:  $\text{SHIFTREG}()$ 
20:  $\text{goto start\_loop}$ 
21: end if
22: end for
23: end for
24: end for

1: procedure  $\text{SPIKE}(\text{row}, \text{flag})$ 
2: if  $\text{row} == \text{currentRow}$  then
3: if  $\text{flag} == 1$  then
4:  $\text{sendSpikeEast}()$ 
5: else
6:  $\text{sendSpikeWest}()$ 
7: end if
8: else
9: if  $\text{flag} == 1$  then
10:  $\text{sendSpikeSouth}()$ 
11: else
12:  $\text{sendSpikeNorth}()$ 
13: end if
14: end if
15: end procedure

1: procedure  $\text{SHIFTREG}$ 
2: if  $m > 0$  then
3: for  $i = 0$  to  $N_{depth} - 2$  do
4:  $\text{Reg}[i] = \text{Reg}[i+1]$ 
5: end for
6:  $m = m - 1$ 
7: end if
8: end procedure

1: RestartUnit(Input: b)
2: if  $\text{Token} == 1$  then
3:  $\text{FlagToken} = 1$ 
4: if  $\text{Reg}[b] == 1$  then
5:  $\text{requestSpike}()$ 
6: for  $t = b$  to  $N_{depth}$  do
7: if  $(S = \text{getSpike}()) \neq \text{NULL}$  then
8:  $\text{Dir} = \text{rotate}(S)$ 
9:  $\text{correctQubit}(\text{Dir})$ 
10:  $\text{sendSyndrome}(\text{Dir})$ 
11: end if
12: if  $t \neq b$  &&  $\text{Reg}[t] == 1$  then
13:  $\text{sendController}(\text{"Finish"})$ 
14: end if
15: end for
16: else
17:  $\text{sendController}(\text{"Finish"})$ 
18: end if
19: else
20: for  $t = b$  to  $N_{depth}$  do
21: if  $\text{Reg}[t] == 1$  then
22:  $\text{SPIKE}(\text{self.row}, \text{FlagToken})$ 
23: if  $\text{getCorrect}()$  then
24:  $\text{Reg}[t] = 0$ 
25:  $\text{sendController}(\text{"Finish"})$ 
26: end if
27: else
28: if  $(S = \text{getSpike}()) \neq \text{NULL}$  then
29:  $\text{Dir} = \text{rotate}(S)$ 
30:  $\text{SPIKE}(\text{self.row}, \text{FlagToken})$ 
31: if  $\text{getCorrect}()$  then
32:  $\text{correctQubit}(\text{Dir})$ 
33:  $\text{sendSyndrome}(\text{Dir})$ 
34: end if
35: end if
36: end if
37: end for
38: end if

```

of qubits on the error syndrome (Fig. 2(b)). The Syndrome signal is passed toward a Unit that initiates the Spike using the saved direction in Step 3) (corresponding to $\text{correctQubit}()$ and $\text{sendCorrect}()$ in Algorithm 1).

This algorithm ensures to find the closest Unit pairs whose Reg values are both 1 by sending a Syndrome signal to the initiator of the first coming Spike. However, this does not necessarily find a set of pairs that minimize the total distance since the sink node is sequentially allocated to Units. Therefore, we limit the maximum number of hops to propagate a Spike in a single run of the above steps and increase it iteratively. The *Controller* procedure in Algorithm 1 implements this by setting a timeout after giving the Token to a Unit.

If an error syndrome appears from one of the Units in the SC toward the outside (Fig. 2(c)), there is no proper matching pair between erroneous ancilla bits. To deal with such a case, we introduce additional Units called *Boundary Units* at the edges of the SC. The

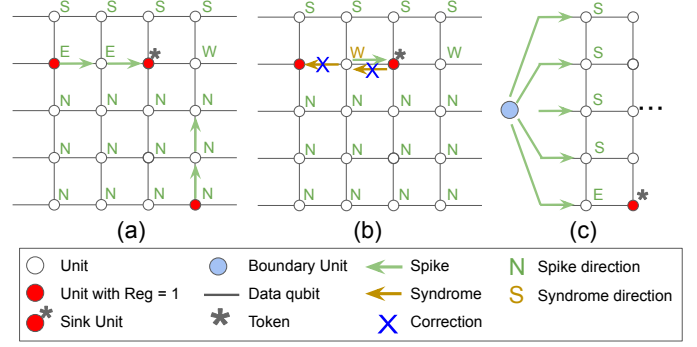


Fig. 2. Overview of the processing of our algorithm.

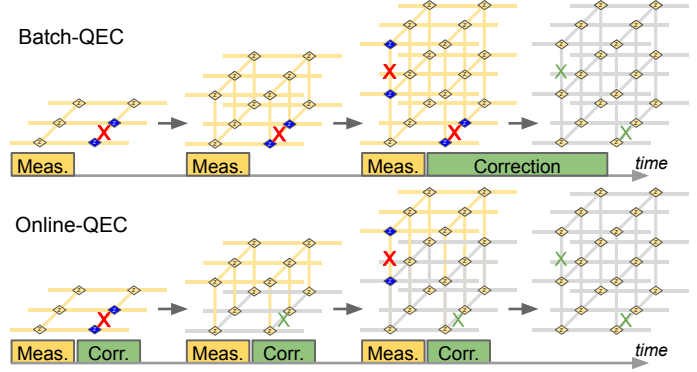


Fig. 3. Concept of Batch- and Online-QEC

Boundary Units never get a Token from the Controller, but always send a Spike upon a $\text{requestSpike}()$ call¹⁾.

To deal with matching problems on a 3-D lattice, results of multiple rounds of measurement for an ancilla bit are stored in each Unit instead of actually having Units for every 3-D lattice points. *Reg* is extended to be an array to hold several measurement results. For every new measurement, the value of the ancilla bit is XORed with the latest value stored in *Reg* (*MeasureEachUnit* process in Algorithm 1).

B. Online-QEC for faster error correction cycle

Figure 3 compares the concepts of batch and online-QEC for a distance-3 SC with measurement errors. In batch-QEC, an error correction phase can be scheduled after three measurements are processed. On the contrary, an error correction phase is associated with each measurement step in online-QEC. This helps correct qubit errors as soon as they occur, which reduces the number of qubit errors in a single QEC phase and makes the matching process easy. However, QEC with only a single SC plane should be avoided due to the occurrence of ancilla bit measurement errors. Hence, the Controller waits for several measurements have done before starting a QEC phase. This is ensured by having at least th_v measurement results in *Reg* for each Unit (L.9 in *Controller* code in Algorithm 1). The threshold value of th_v controls a trade-off between the error-to-correction latency and error correction performance. We evaluate the appropriate th_v in the next Subsection.

In the Spike generation, multiple bits in a *Reg* are sought step-by-step from the oldest to the newest measurement. Once a non-sink Unit finds the value of 1 in the current bit position, it sends a Spike to the sink Unit. This process is repeated by changing the *base depth*

¹⁾To prioritize matching between normal Units, the Spike timing of Boundary Units is adjusted in the implementation.

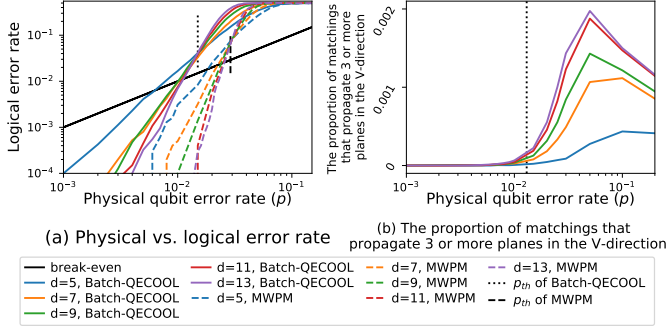


Fig. 4. (a) Error rate scaling for the MWPM decoder and batch-QECCOL. We can observe the threshold value of QECCOL at approximately 1.5% physical error rate. (b) The proportion of matchings that propagate through three or more planes in the vertical direction.

which points to the start position of the Reg for seeking. Otherwise, the matching process is the same as the 2-D case.

C. Necessary vertical depth for online-QEC

We evaluate how the vertical depth threshold th_v affects the error correction performance of QECCOL. We perform a spike-based QEC shown in Algorithm 1 with the batch-QEC manner by setting N_{depth} and th_v to d and -1 , respectively, indicating that the Controller process is executed after d times measurement. We call this method as *batch-QECCOL*.

The error-correcting performance is evaluated numerically by a quantum error simulator. We simulate the QECCOL algorithm with both informational and ancilla qubit errors using the phenomenological noise model [4]. We show logical X error rates versus physical Pauli- X error rate as the performance indicator²⁾. We assume the error probabilities of data and ancilla qubits are equal. Note that the same experimental setup is used in Section V-B.

Figure 4(a) shows the log scale plots of physical qubit error rate and logical- X error rate for Pauli- X errors. The solid black line is the break-even (physical error rate = logical error rate) value. The other solid lines show the results for batch-QECCOL, whereas the dashed lines represent cases for MWPM [7].

We use *threshold values* to evaluate the error correction performance of our algorithm. The threshold value, p_{th} , is defined for each decoding algorithm and represents the value of physical error rate p that satisfies the following properties; if the physical error rate p is less than p_{th} , the logical error rate p_L decreases as the code distance d increases. It can be defined as the value of p at the intersection of p and p_L plotted for several code distances d . The higher the p_{th} , the better the decoding algorithm. p_{th} of batch-QECCOL can be obtained from Fig. 4(a) and it is around $p = 0.015$, while that of MWPM is 0.03.

Figure 4(b) shows the proportion of matchings that propagate through three or more planes in the vertical (temporal) direction on a 3-D lattice. While three or more propagation in the vertical direction happens many times in larger physical error rate p , it is negligible for relatively smaller p , especially when p is less than p_{th} . In general, QEC decoders require that the physical error rate p is smaller than their p_{th} for realistic error correction. This indicates having three SC planes (or Reg of three entries in QECCOL) for online-QEC is almost satisfactory. Thus, we assume $th_v = 3$ in the following sections.

²⁾Under the assumption that Pauli X , Y , and Z errors occur stochastically, Y errors can be considered as a simultaneous X and Z error. Therefore, even if X and Z errors are corrected independently, all errors can be decoded correctly. Thus, we show only the case of X error.

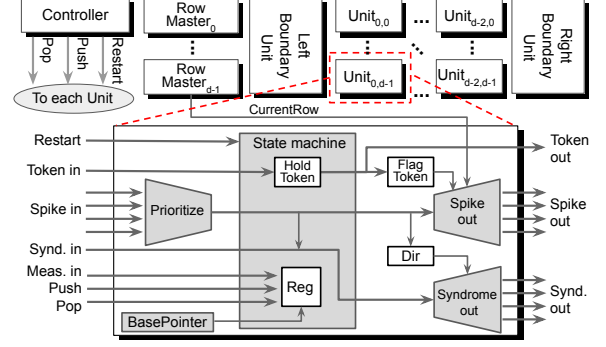


Fig. 5. Overview of the architecture and the microarchitecture of Unit

IV. HARDWARE IMPLEMENTATION

A. Hardware architecture

Figure 5 shows the overview of the hardware architecture for X error detection for a single distance- d logical qubit³⁾. Each hardware Unit corresponds to the “Unit” of Algorithm 1, and $d \times (d - 1)$ Units are aligned in a 2-D grid pattern. There is one Controller per one logical qubit to orchestrate the Units by distributing *Push*, *Pop*, and *Restart* signal. Note that this architecture can be easily extended to any code distance d thanks to its distributed nature.

Each Unit has a register (Reg) that stores measured values of the corresponding ancilla bit. It works as a queue; whenever the measurement process is performed, the Controller sends the *Push* signal to all the Units and the measured value is stored at the end of Reg. When the first bit entry of Reg (corresponding to the oldest measurement) of all the Units becomes 0, the error correction process for the current layer is completed. In this case, the Controller broadcasts the *Pop* signal, which makes the values in the Reg being one-bit shifted. Based on the results of Section III-C, we assume $th_v = 3$ which means the Reg needs to store at least three measurement values. In this paper, we set the size of a Reg to 7-bit with some margin.

A “Row Master” module is attached to each row of the 2-D Unit array and gives the Token to the first Unit of the row. It always checks Reg values in all the Units in the row, and if none of the bits in Reg is 1, it avoids giving the Token to the row to avoid meaningless Token passing on non-erroneous Units which helps reduce the time taken for QEC. In this case, it just passes the Token to the next Row Master. It is also responsible to send *CurrentRow* signal to all the Units of the row.

Two *Boundary Units* are located on each side of the Unit array. Each of them is connected to d Units on a horizontal edge. One Boundary Unit can be shared by all the Units on each edge. Distributing a Spike to all the Units does not affect QEC’s correctness since only the first Spike that reaches the Sink Unit is valid in the algorithm.

B. Unit implementation

In each Unit, there are five components as described below.

- **State machine:** A state machine controls the behavior of the Unit. The state transition happens based on *Restart* signal, coming *Token*, and coming *Spike*. This module has two register memories; *HoldToken* and *Reg*, and their values affect state transition.
- **Prioritization module:** As a Unit may get multiple Spikes from different directions simultaneously, we need to prioritize the input from a specific direction. This module selects one Spike from them by the predefined priority. We use the race logic concept, which utilizes the relative propagation time of signals. We put an

³⁾The identical hardware applies to Z error detection.

TABLE I
SUMMARY OF SFQ LOGIC ELEMENTS

cell	JJs	Bias current (mA)	Area (μm^2)	Latency (ps)
splitter	3	0.300	900	4.3
merger	7	0.880	900	8.2
1:2 switch	33	3.464	8100	10.5
destructive readout (DRO)	6	0.720	900	5.1
nondestructive readout (NDRO)	11	1.112	1800	6.4
resettable DRO (RD)	11	0.900	1800	6.0
dual-output DRO (D2)	12	0.944	1800	6.8

appropriate signal delay in each direction for coming Spike so that a Spike from the highest priority direction must come faster than the others.

- **Spike out module:** This module sends a Spike to the appropriate direction based on values of the CurrentRow and the FlagToken.
- **Syndrom out module:** This module sends a Syndrome signal to the direction indicated by the *Dir* register that stores the opposite direction of the coming Spike. It also generates a correction signal to the associated data qubit.
- **BasePointer module:** This module controls which bit position in Reg to be read out based on the value of the base register. The read value from Reg is used to decide whether the Unit should send a Spike.

C. SFQ logic gates

We designed the QECOOL hardware based on an RSFQ cell library [22] developed for a niobium nine-layer, 1.0- μm fabrication technology [9], [15]. Table I summarizes the SFQ logic gates used in this work. Since the essential element of SFQ that affects power consumption and hardware cost is Josephson junction (JJ), the Table shows the number of JJs for each gate and assumed the bias current required for operation. The operating temperature and designed supply voltage are 4-K and 2.5 mV, respectively. In RSFQ, since most of the power is consumed statically almost independent of switching activities, it is calculated by multiplying the bias voltage and currents.

TABLE II

THE TOTAL NUMBER OF LOGIC ELEMENTS, THE NUMBER OF JJs, CIRCUIT AREA AND THE OF EACH MODULE THAT CONSTITUTES AN ANCILLA UNIT BASED ON THE AIST 10-KA/CM² ADP CELL LIBRARY [22].

cell	State machine	Prioritization	Base pointer (7-bit)	Spike out	Syndrom out	Other	Total (7-bit)
splitter	17	4		8		2	31
merger	14	9	30	8	2	2	65
1:2 switch	8		3	3			11
DRO			20				20
NDRO			30	4	4		44
RD	6		6				6
D2			1085	91		18	1472
Wire	196	82					
Total JJs	675	157	1935	314	58	38	3177
Total area (μm^2)	265500	82800	709200	129600	25200	62100	1274400
Total bias current (mA)	69.7	15.3	208.5	32.2	5.4	5.0	336
Latency (ps)	98.7	28.0	147	61.1	10.4		215

We used the Josephson simulator (JSIM) [6], a SPICE-level simulator, to verify the functionality of the designed Unit with 7-bit Reg and evaluate its latency. Table II shows the total number of JJs, total area, total bias current, and latency of each module. Figure 6 shows the layout of the QECOOL Unit. A Unit consists of 3177 JJs in total, and its area footprint is 1.274 mm². The maximum delay of the designed circuit is 215 ps, results in the maximum operating frequency of about 5 GHz. It can operate fast enough to achieve the required QEC latency described later in Section V-A. The power consumption of a Unit is $336_{[\text{mA}]} \times 2.5_{[\text{mV}]} = 840_{[\mu\text{W}]}$ including the wiring power, if implemented with RSFQ logic.

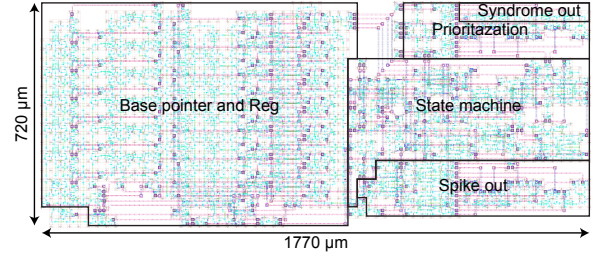


Fig. 6. The layout of the designed QECOOL Unit

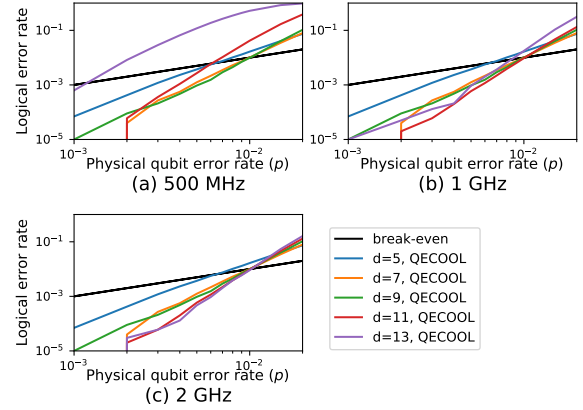


Fig. 7. Physical vs. logical error rate plot for the QECOOL algorithm operating at several frequencies.

V. EVALUATIONS OF THE ONLINE-QEC DECODER

A. Execution cycles

TABLE III
PER LAYER EXECUTION CYCLES OF QECOOL

<i>d</i>	<i>p</i> = 0.001			<i>p</i> = 0.005			<i>p</i> = 0.01		
	Max	Avg	σ	Max	Avg	σ	Max	Avg	σ
5	104	6.10	4.99	144	10.4	11.2	166	15.6	15.8
7	303	11.8	14.5	515	28.7	30.1	557	47.4	43.9
9	800	22.7	30.6	1018	64.2	57.7	1308	107	89.7
11	996	41.6	53.6	1779	120	95.3	2435	201	161
13	1890	71.3	82.9	3289	199	147	4072	337	266

Table III shows the number of execution cycles per layer for QECOOL for several combinations of coding distance *d* and physical error rate *p*. It is observed that the execution cycles of QECOOL are highly dependent on *d* and *p*.

Since it is reported that measuring ancilla bit takes about 1 μs [10], QEC is fast enough if the process for one layer is finished within 1 μs .

B. Error correction performance

We use the same error model as in Subsection III-C to evaluate the performance of QECOOL for online-QEC. The measurement process is assumed to be performed once every 1 μs . Each Unit has 7-bit Reg, and th_v in Algorithm 1 is set to 3. If Reg overflows because of the slow QEC performance, the trial is considered as a failure.

Figures 7(a) and (b) indicate that the slower frequency causes buffer overflow of Unit, which affects the error correction performance at larger code distance *d*. Only in Figure 7(c), we can observe the p_{th} of QECOOL at approximately $p = 1.0\%$, which is slightly smaller than that of batch-QECOOL.

C. Power estimation with ERSFQ logic

To put the more decoder units in a dilution refrigerator, their power consumption should be much lower, and the RSFQ technology is not

TABLE IV
QUALITATIVE COMPARISON OF DECODER PERFORMANCE

Decoder	P_{th} (2-D / 3-D)	Latency	Environment
MWPM [7]	10.3% / 2.9%	High	Software
UF [3]	9.9% / 2.6%	Medium	FPGA [2]
AQEC [11]	5% / -	Very low	SFQ
QECOOL	6.0% / 1.0%	Low	SFQ

TABLE V
COMPARISON OF AQEC [11] AND QECOOL

	p_{th} (2-D/3-D)	Execution time per layer (Max/Avg.) (ns)	Power per Unit (μW)	# Units required per logical qubit	Directly appli- cable to 3-D	# protect- able logical qubits
AQEC	5.0% / -	19.8 / 3.93	13.44	$(2d-1)^2$	No	37
QECOOL (7-bit Reg)	6.0% / 1.0%	400 / 20.8	2.78	$2d(d-1)$	Yes	2498

feasible. Instead, we need to use the ERSFQ [13] technology where the static power consumption is eliminated. Power consumption in ERSFQ circuits is only consumed by dynamic power twice as high as that of RSFQ. Though ERSFQ is slower than RSFQ, this is not a problem for our hardware design since our target clock frequency is much lower than the maximum frequency in RSFQ.

Based on the RSFQ design and the power model of ERSFQ [14], we estimate the power consumption when ERSFQ is applied. Here, the power of a Unit with ERSFQ can be estimated as follows:

$$P_{unit} = (\text{bias current}) \times (\text{frequency}) \times \Phi_0 \times 2$$

We use flux quantum Φ_0 of 2.068×10^{-15} Wb. The reason why it is multiplied by 2 is to represent twice of dynamic power in ERSFQ.

For a proposed Unit with 7-bit Reg, the total bias current is 336 mA. If we suppose 2 GHz clock frequency, the power consumption of a Unit at a 4-K environment is estimated as follows:

$$336_{\text{[mA]}} \times 2_{\text{[GHz]}} \times (2.068 \times 10^{-15})_{\text{[Wb]}} \times 2 = 2.78_{\text{[}\mu\text{W/Unit]}}$$

D. Comparison to existing decoders

Table IV shows a brief comparison of MWPM and recent prominent hardware-efficient decoding algorithms. While MWPM and union-find (UF) have a higher threshold, they are designed to operate in a room-temperature environment as they are implemented by software or an FPGA device.

AQEC [11] and our decoder are designed to operate in a cryogenic environment and have higher scalability than others, though these have a slightly lower threshold. We summarize a detailed comparison of AQEC and QECOOL in Table V. We assume the coding distance d of 9, the longest one evaluated in the AQEC paper, and the physical error rate (for both data and ancilla qubits) p of 0.001, which is 0.1 times the p_{th} of our decoder. The power budget of the 4-K temperature region of dilution refrigerators is supposed to be 1 W [12], and the number of protectable qubits is estimated in terms of the decoders' power consumption. Applying the same arguments as Subsection III-C, we assume that extending AQEC to 3-D requires 7 times the modules needed for 2-D processing. In addition, we optimistically consider AQEC's latency for 2-D processing as its per layer latency when extended to 3-D. The Table shows that QECOOL is superior to AQEC in other aspects than latency, which is not a major disadvantage since our decoder can finish one layer process within 1 μ s, the interval of the measurement process [10]. AQEC can lower its operating frequency to reduce its power consumption by taking advantage of its low latency, however, our method still has lower power consumption, even taking this into account. Note that the p_{th} of AQEC for the 3-D case is unknown, and it is expected to be slightly smaller than ours as the p_{th} trends of 2-D to 3-D in Table IV indicate 70-80% reduction in 3-D cases.

VI. CONCLUSION

In this paper, we proposed an online-QEC algorithm named QECOOL for decoding surface code with measurement errors and designed a decoder with SFQ logic based on the algorithm. We evaluated the circuit characteristics and the error-correcting performance of our design. As a result, our decoder is power-efficient enough to protect around 2500 logical qubits with distance-9 surface code in the 4-K layer of a dilution refrigerator, and it is fast and accurate enough for online-QEC.

REFERENCES

- [1] F. Arute et al. Quantum supremacy using a programmable superconducting processor. *Nature*, 574(7779):505–510, 2019.
- [2] P. Das et al. A scalable decoder micro-architecture for fault-tolerant quantum computing. *arXiv preprint arXiv:2001.06598*, 2020.
- [3] N. Delfosse and N. H. Nickerson. Almost-linear time decoding algorithm for topological codes. *arXiv preprint arXiv:1709.06218*, 2017.
- [4] E. Dennis, A. Kitaev, A. Landahl, and J. Preskill. Topological quantum memory. *Journal of Mathematical Physics*, 43(9):4452–4505, 2002.
- [5] D. E. Drake and S. Hougardy. A simple approximation algorithm for the weighted matching problem. *Information Processing Letters*, 85(4):211–213, 2003.
- [6] E. S. Fang and T. Van Duzer. A josephson integrated circuit simulator (JSIM) for superconductive electronics application. In *Extended Abstracts of 1989 International Superconductivity Electronics Conference*, pages 407–410, 1989.
- [7] A. G. Fowler. Minimum weight perfect matching of fault-tolerant topological quantum error correction in average $O(1)$ parallel time. *Quantum Info. Comput.*, 15(1–2):145–158, 2015.
- [8] A. G. Fowler, M. Mariantoni, J. M. Martinis, and A. N. Cleland. Surface codes: Towards practical large-scale quantum computation. *Phys. Rev. A*, 86:032324, 2012.
- [9] A. Fujimaki et al. Large-scale integrated circuit design based on a Nb nine-layer structure for reconfigurable data-path processors. *IEICE Transactions on Electronics*, E97.C(3):157–165, 2014.
- [10] C. Gidney and M. Eker. How to factor 2048 bit rsa integers in 8 hours using 20 million noisy qubits. *arXiv: Quantum Physics*, 2019.
- [11] A. Holmes, M. R. Jokar, G. Pasandi, Y. Ding, M. Pedram, and F. T. Chong. NISQ+: Boosting quantum computing power by approximating quantum error correction. In *Proceedings of the ACM/IEEE 47th Annual International Symposium on Computer Architecture*, page 556–569, 2020.
- [12] J. M. Hornibrook et al. Cryogenic control architecture for large-scale quantum computing. *Phys. Rev. Applied*, 3:024010, 2015.
- [13] D. E. Kirichenko, S. Sarwana, and A. F. Kirichenko. Zero static power dissipation biasing of RSFQ circuits. *IEEE Transactions on Applied Superconductivity*, 21(3):776–779, 2011.
- [14] O. A. Mukhanov. Energy-efficient single flux quantum technology. *IEEE Transactions on Applied Superconductivity*, 21(3):760–769, 2011.
- [15] S. Nagasawa et al. Nb 9-layer fabrication process for superconducting large-scale SFQ circuits and its process evaluation. *IEICE Transactions on Electronics*, E97.C(3):132–140, 2014.
- [16] R. Sato et al. High-speed operation of random-access-memory-embedded microprocessor with minimal instruction set architecture based on rapid single-flux-quantum logic. *IEEE Transactions on Applied Superconductivity*, 27(4):1300505, 2017.
- [17] P. W. Shor. Scheme for reducing decoherence in quantum computer memory. *Physical review A*, 54(4):R2493, 1995.
- [18] P. W. Shor. Polynomial-time algorithms for prime factorization and discrete logarithms on a quantum computer. *SIAM Journal on Computing*, 26(5):1484–1509, 1997.
- [19] S. S. Tannu, D. M. Carmean, and M. K. Qureshi. Cryogenic-dram based memory system for scalable quantum computers: A feasibility study. In *Proceedings of the International Symposium on Memory Systems*, page 189–195, 2017.
- [20] S. S. Tannu, Z. A. Myers, P. J. Nair, D. M. Carmean, and M. K. Qureshi. Taming the instruction bandwidth of quantum computers via hardware-managed error correction. In *2017 50th Annual IEEE/ACM International Symposium on Microarchitecture*, pages 679–691, 2017.
- [21] S. Varsamopoulos, K. Bertels, and C. G. Almudever. Comparing neural network based decoders for the surface code. *IEEE Transactions on Computers*, 69(2):300–311, 2019.
- [22] Y. Yamanashi et al. 100 GHz demonstrations based on the single-flux-quantum cell library for the 10 kA/cm² Nb multi-layer process. *IEICE Transactions on Electronics*, 93(4):440–444, 2010.